19. Dejana E, Orsenigo F, Lampugnani MG (2008) The role of adherens junctions and VE-cadherin in the control of vascular permeability. J Cell Sci 121:2115–2122. doi:10.1242/jcs.017897
20. Nakamuta S, Endo H, Higashi Y, Kousaka A, Yamada H et al (2008) Human immunodeficiency virus type 1 gp120-mediated disruption of tight junction proteins by induction of proteasome-mediated degradation of zonula occludens-1 and -2 in human brain microvascular endothelial cells. J Neurovirol 14:186–195. doi:10.1080/13550280801993630
21. Dewi BE, Takasaki T, Kurane I (2008) Peripheral blood mononuclear cells increase the permeability of dengue virus-infected endothelial cells in association with downregulation of vascular endothelial cadherin. J Gen Virol 89:642–652. doi:10.1099/vir.0.83356-0
22. Liao CK, Jeng CJ, Wang HS, Wang SH, Wu JC (2013) Lipopolysaccharide induces degradation of connexin43 in rat astrocytes via the ubiquitin-proteasome proteolytic pathway. PLoS One 8(11):e79350. doi:10.1371/journal.pone.0079350
23. Aberle H, Bauer A, Stappert J, Kispert A, Kemler R (1997) β-Catenin is a target for the ubiquitin-proteasome pathway. EMBO J 16:3797–3804. doi:10.1093/emboj/16.13.3797
24. Xiong S, Mu T, Wang G, Jiang X (2014) Mitochondria-mediated apoptosis in mammals. Protein Cell. doi:10.1007/s13238-014-0089-1
25. Steinhusen U, Badock V, Bauer A, Behrens J, Wittman-Liebold B et al (2000) Apoptosis-induced cleavage of beta-catenin by caspase-3 results in proteolytic fragments with reduced transactivation potential. J Biol Chem 275:16345–16353. doi:10.1074/jbc.M001458200
26. Tran AT, Cortens JP, Du Q, Wilkins JA, Coombs KM (2013) Influenza virus induces apoptosis via BAD-mediated mitochondrial dysregulation. J Virol 87:1049–1060. doi:10.1128/JVI.02017-12
27. Childs EW, Tharakan B, Hunter FA, Tinsley JH, Cao X (2007) Apoptotic signaling induces hyperpermeability following hemorrhagic shock. Am J Physiol Heart Circ Physiol 292:H3179–H3189. doi:10.1152/ajpheart.01337.2006
28. Tharakan B, Hellman J, Sawant DA, Tinsley JH, Parrish AR et al (2012) β-Catenin dynamics in the regulation of microvascular endothelial cell hyperpermeability. Shock 37:306–311. doi:10.1097/SHK.0b013e318240b564
29. Mariappan N, Elks CM, Fink B, Francis J (2009) TNF-induced mitochondrial damage: a link between mitochondrial complex I activity and left ventricular dysfunction. Free Radic Biol Med 46:462–470. doi:10.1016/j.freeradbiomed.2008.10.049
30. Mizuguchi M, Yamanouchi H, Ichiyama T, Shiomi M (2007) Acute encephalopathy associated with influenza and other viral infection. Acta Neurol Scand 115:45–56. doi:10.1111/j.1600-0404.2007.00809.x
31. Zhang P, Katz J, Michalek SM (2009) Glycogen synthase kinase-3β (GSK3β) inhibition suppress the inflammatory response to *Francisella* infection and protects against tularemia in mice. Mol Immunol 46:677–687. doi:10.1016/j.molimm.2008.08.281
32. Tay TF, Maheran M, Too SL, Hasidah MS, Ismail G et al (2012) Glycogen synthase kinase-3β inhibition improved survivability of mice infected with *Burkholderia pseudomallei*. Trop Biomed 29:551–567
33. Chang YT, Chen CL, Lin CF, Lu SL, Cheng MH, Kuo CF, Lin YS (2013) Regulatory role of GSK-3β on NF-κB, nitric oxide, and TNF-α in group A streptococcal infection. Mediators Inflamm 2013:720689. doi:10.1155/2013/720689
34. Pauligk C, Nain M, Reiling N, Gemsa D, Kaufmann A (2004) CD14 is required for influenza A virus-induced cytokine and chemokine production. Immunobiology 209:3–10. doi:10.1016/j.imbio.2004.04.002

PLOS | ONE

RESEARCH ARTICLE

Abbreviated Half-Lives and Impaired Fuel Utilization in Carnitine Palmitoyltransferase II Variant Fibroblasts

Min Yao[1,2☯], Min Cai[1☯], Dengfu Yao[2], Xi Xu[2], Rongrong Yang[2], Yuting Li[1], Yuanyuan Zhang[2], Hiroshi Kido[3], Dengbing Yao[1]*

1 School of Life Sciences, Key Laboratory of Neuroregeneration, Co-innovation Center of Neuroregeneration, Nantong University, Nantong, Jiangsu, P. R. China, **2** School of Medicine, Affiliated Hospital of Nantong University, Nantong, Jiangsu, P. R. China, **3** Division of Enzyme Chemistry, Institute for Enzyme Research, the University of Tokushima, Tokushima, Japan

☯ These authors contributed equally to this work.
* yaodb@ntu.edu.cn

OPEN ACCESS

Citation: Yao M, Cai M, Yao D, Xu X, Yang R, Li Y, et al. (2015) Abbreviated Half-Lives and Impaired Fuel Utilization in Carnitine Palmitoyltransferase II Variant Fibroblasts. PLoS ONE 10(3): e0119936. doi:10.1371/journal.pone.0119936

Received: July 18, 2014

Accepted: January 28, 2015

Published: March 17, 2015

Data Availability Statement: All relevant data are within the paper and its Supporting Information files.

Funding: This research was supported by grants from: National Natural Science Foundation of China (Grant No. 81370982, 81200634); Scientific Research Foundation for Returned Scholars, Ministry of Education of China; Natural Science Foundation of Jiangsu Province (Grant No. BK2010282) and A Project Funded by the Priority Academic Program Development of Jiangsu Higher Education Institutions, PAPD. The funders had no role in study design, data collection and analysis, decision to publish, or preparation of the manuscript.

Competing Interests: The authors have declared that no competing interests exist.

Abstract

Carnitine palmitoyltransferase II (CPT II) deficiency is one of the most common causes of fatty acid oxidation metabolism disorders. However, the molecular mechanism between *CPT2* gene polymorphisms and metabolic stress has not been fully clarified. We previously reported that a number of patients show a thermal instable phenotype of compound hetero/homozygous variants of CPT II. To understand the mechanism of the metabolic disorder resulting from CPT II deficiency, the present study investigated CPT II variants in patient fibroblasts, [c.1102 G>A (p.V368I)] (heterozygous), [c.1102 G>A (p.V368I)] (homozygous), and [c.1055 T>G (p.F352C)] (heterozygous) + [c.1102 G>A (p.V368I)] (homozygous) compared with fibroblasts from healthy controls. CPT II variants exerted an effect of dominant negative on the homotetrameric proteins that showed thermal instability, reduced residual enzyme activities and a short half-life. Moreover, CPT II variant fibroblasts showed a significant decrease in fatty acid β-oxidation and adenosine triphosphate generation, combined with a reduced mitochondrial membrane potential, resulting in cellular apoptosis. Collectively, our data indicate that the CPT II deficiency induces an energy crisis of the fatty acid metabolic pathway. These findings may contribute to the elucidation of the genetic factors involved in metabolic disorder encephalopathy caused by the CPT II deficiency.

Introduction

The carnitine palmitoyl-transferase (CPT) system is component of adenosine triphosphate (ATP) production through fatty acid β-oxidation [1–7]. It consists of two enzymes CPT I and CPT II which located in the mitochondrial membranes. The CPT system transfers long chain fatty acids from cytosol to mitochondrial. The rate-limiting step in the transfer of long chain fatty acid is that CPT I transesterificates acyl-CoA to acylcarnitine [8, 9], but CPT II changes

acylcarnitine to acyl-CoA. The CPT II protein is a homotetramer encoded by *CPT2* gene which located on chromosome 1p32, contains five exons ranging from 81 to 1,305 bp in size. Fatty acid metabolized by β-oxidation pathway represents energy source performed particular in muscle and also in nerve system. The autonomic recessive CPT II deficiency is the inherited disease of the mitochondrial long chain fatty acid oxidation, includes a severe infantile hepatocardiomuscular form, a lethal neonatal form, and a myopathic form [10–14].

To date, more than 70 different mutations of *CPT2* have recently been reported, and studies have demonstrated the relationships between the CPT II deficiency genotypes and their clinical phenotypes characterized by febrile convulsions and multiple-organ failure during high fever [15–21]. However, the molecular mechanism underlying the relationship between *CPT2* polymorphisms and metabolic stress has not been completely clarified. Previously, we have reported that a number of influenza-associated encephalopathy patients exhibit a thermolabile phenotype of compound hetero/homozygous variants of CPT II [20–22], and analyzed the enzymatic properties of CPT II variants expressed in transfected COS-7 cells. The direct biochemical consequences of the mutations are still controversial. To understand the mechanisms of the metabolic disorder resulting from CPT II deficiency, we studied CPT II variants in patient fibroblasts, [c.1102 G>A (p.V368I)] (heterozygous), [c.1102 G>A (p.V368I)] (homozygous), and [c.1055 T>G (p.F352C)] (heterozygous) + [c.1102 G>A (p.V368I)] (homozygous) compared with control fibroblasts. Our study hypothesis was that the CPT II deficiency caused a lack of enzymatically active CPT II protein and induced an energy crisis in the fatty acid metabolic pathway. Our findings may contribute to the elucidation of the genetic factors involved in metabolic disorder encephalopathy.

Materials and Methods

Materials

[1-^{14}C] oleic acid, L-[methyl-^{3}H] carnitine, L-[^{35}S] methionine, and enhanced chemiluminescence detection reagents were bought from Amersham Pharmacia Biotech (Piscataway, NJ, USA), the BCA reagent was from Pierce (Rockford, IL, USA). The ABI DyeDeoxy Terminator Cycle Sequencing Kit was obtained from PE-Applied Biosystems (Foster City, CA, USA).

CPT II deficiency patients and *CPT2* polymorphism analysis

This study was approved by the Ethics Review Committee for human genome analysis of the Key Laboratory of Neuroregeneration, Nantong University. Informed written consents were obtained from the adult patients and from the next of kin, caretakers, or guardians on behalf of the minor patients in this study. To diagnose CPT II deficiency, patient plasma was examined to determine the accumulation of long-chain acylcarnitines, which is indicative of disease. A total of 12 patients were diagnosed with CPT II deficiency on the basis of clinical manifestations, including the abrupt onset of seizures and coma developing within 12–48 h after the onset of high fever (≥40°C). In all patients, the age range was from 1 to 56 years, eight patients were males and four were females. To confirm the diagnosis, *CPT2* mutation analysis was performed by PCR-amplifying the five coding exons and flanking intronic regions of *CPT2* from genomic DNA extracted from EDTA—whole blood. The primers were intronic (S1 Table), and have been described previously [20–23]. PCR products were sequenced directly by using ABI-PRISM 3100 Genetic Analyzer. The PCR products were sequenced in both strands and the analysis were performed in triplicate. The sequencing results showed the following mutations: NM_000098.2 (CPT2_v001): [c.1102 G>A (p.V368I)] (heterozygous), and [c.1102 G>A (p.V368I)] (homozygous), [c.1055 T>G (p.F352C)] (heterozygous) + [c.1102 G>A (p.V368I)] (homozygous).

Assay of CPT II activity and kinetic properties

We collected the fibroblasts of CPT II variations with clinical symptoms and biochemical markers characteristic of this inherited metabolic disorder. The control fibroblasts were bought from company. These fibroblasts were cultured at 37°C in 5% CO_2 in Dulbecco's modified Eagle's medium (DMEM) containing 10% fetal serum (Indianapolis, IN, USA). CPT II activities in the fibroblast lysates were measured at 30°C for 2 h, by detection of palmitoyl-L-[methyl-^{3}H] carnitine formed from L-[methyl-^{3}H] carnitine and palmitoyl-CoA [6]. The palmitoyl-L-[methyl-^{3}H] carnitine formed was extracted and radioactivity levels were counted. The V_{max} and K_m values were analyzed by measuring the enzyme activity at 30°C by varying the L-[methyl-^{3}H] carnitine concentrations. To analyze the heat stability of control and CPT II deficiency fibroblasts, cell lysates were pre-incubated at conditions simulating a high fever (41°C) or stable conditions (30°C) for 0–2 h, and the enzyme activities were assayed after the addition of 200 μM L-[methyl-^{3}H] carnitine then continue incubated at 30°C for 2 h [20–23]. The protein concentrations in the fibroblast lysates were assayed using the bicinchoninic acid protein assay reagent kit.

Expression of control and patient *CPT2* mRNA

To analyze *CPT2* mRNA expression levels of control and patient fibroblasts, total RNA was extracted using the RNeasy Mini Kit. The fibroblasts cDNA were synthesized using a random primer and reverse transcriptase. The expression of *CPT2* mRNA levels was analyzed by real-time quantitative PCR with *CPT2*-specific primers.

CPT II protein expression of control and patient fibroblasts was analyzed by sodium dodecyl sulfate polyacrylamide gel electrophoresis (SDS-PAGE) under reducing conditions, followed by Western Blotting with anti-CPT II antibodies. The amount of CPT II total RNA and proteins were expressed relative to those of β-actin control.

Mitochondrial membrane potential analysis

Fibroblasts were cultured for 5 h at 37°C or 41°C and then continue incubated for an another 15 min with 5,5′, 6,6′-Tetrachloro-1,1′,3,3′-tetraethylbenzimidazolyl-carbocyanineiodide fluorescent dye (JC-1) from the Probes in the dark. Then they were washed with assay buffer and immediately imaged with the red fluorescence channel ($\lambda_{excitation}$: 560 ± 40 nm band pass filter, $\lambda_{detection}$: 630 ± 60 nm band pass filter) using a fluorescence microscope and with the green fluorescence channel ($\lambda_{excitation}$: 470 ± 40 nm band pass filter, $\lambda_{detection}$: 535 ± 50 nm band pass filter) [20, 21].

Apoptosis analysis of CPT II variants

The percentage of apoptotic control and patient fibroblasts was measured by flow cytometry. Annexin V—FITC was added to cell suspensions following propidium iodide labelling, and the number of apoptotic fibroblasts was counted by FACScan flow cytometry according to the manufacturer's protocol and based on an annexin V flow cytometry histogram. Fibroblasts incubated with dimethyl sulfoxide (DMSO) were used as a control. Control and patient fibroblasts were also analyzed by a lactate dehydrogenase (LDH) cytotoxicity assay. The LDH reagent and catalyst was added to the supernatant from fibroblast medium and incubated for 30 min at room temperature. The absorbance was recorded at 490 nm with background subtraction at 630 nm using the Synergy HT multi-detection Micro Plate Reader, and results were shown as a percentage of LDH release. To analyze the apoptotic factor release, fibroblasts were lysed and immunoblotted separately with anti-caspase-3,-caspase-8,-cytochrome c, and-Bid

antibodies. CPT II protein expression levels were expressed relative to those of β-actin. All experiments were carried out in triplicate.

CPT II half-lives of control and patient fibroblasts

Cultured fibroblasts were washed with PBS and incubated for 48 h in serum- and methionine-free medium 30 min, then followed by pulse chase labeling with [^{35}S]-methionine (specific activity 1,000 Ci/mM) for 2 h. After pulse labeling, the fibroblasts were again washed with PBS and chased for 0, 6, 12, and 18 h. At each chase interval, the fibroblasts were lysed and immunoprecipitated with anti-CPT II antibody coupled to Protein G-Sepharose 4B. Then the immunoprecipitates were separated by SDS-PAGE and the dried gels were analyzed autoradiographically [20, 21].

Mitochondrial fatty acid β-oxidation and ATP generation

The β-oxidation of mitochondrial fatty acids was analyzed as previously described by Saudubray et al. [20]. Control and patient fibroblasts were cultured at 37°C or 41°C in plastic center containing a filter paper, then continue cultured for an additional 2 h. At the end of the incubation, the reaction was stopped by the addition of perchloric acid, and the radioactive CO_2 released from the fibroblasts was collected for 1 h at room temperature by injecting NaOH onto the filter paper under slow shaking. The filter papers were retrieved and the amount of $^{14}CO_2$ radioactivity was counted using liquid scintillation counting in ACS II in a Beckman LS 6500 multi-purpose scintillation counter [20].

Fibroblasts were washed twice with PBS and cellular ATP was extracted with 1% trichloroacetic acid, then the ATP production concentration was measured. The extracts were centrifuged and immediately diluted with 1 M Tris-acetate buffer. The total ATP generation in the extracts was measured by an ATP assay system bioluminescence detection kit according to the manufacturer's instructions.

Statistical analysis

The data were statistical analyzed using SPSS 15.0 for windows. The Student's t-test was used for comparison between the groups. $P<0.05$ was considered statistically significant. All data were expressed as mean ± SD.

Results

CPT2 polymorphisms in CPT II deficiency patients

Genotype analyses of *CPT2* in patients suffering from CPT II deficiency identified three polymorphisms associated with amino acid substitutions: [c.1102 G>A (p.V368I)] (heterozygous), [c.1102 G>A (p.V368I)] (homozygous), and [c.1055 T>G (p.F352C)] (heterozygous) + [c.1102 G>A (p.V368I)] (homozygous). These variations matched the mutations previously reported in late-onset muscular, infantile/juvenile hepatic, and severe neonatal phenotypes of CPT II deficiency [24–30]. Mutations [c.1055 T>G (p.F352C)] (heterozygous) + [c.1102 G>A (p.V368I)] (homozygous) are located near the acylcarnitine binding residues [26], and transient serum acylcarnitine ratios [$(C_{16:0} + C_{18:1})/C_2$] of >0.09 were previously observed during high fever. These variations were found not only in disease-causing mutations defined as pathogenic but also found in polymorphisms of *CPT2* gene associated with inherited CPT II deficiency. The three polymorphisms found in *CPT2* gene and in the studied patients [c.1102 G>A (p.V368I)] (heterozygous), [c.1102 G>A (p.V368I)] (homozygous), and [c.1055 T>G (p.F352C)] (heterozygous) + [c.1102 G>A (p.V368I)] (homozygous) matched the mutations

previously reported in late-onset muscular, infantile/juvenile hepatic, and severe neonatal phenotypes of CPT II deficiency.

Enzymatic properties and thermal instability of CPT II variants

We next examined the CPT II activity and kinetic properties of fibroblast lysates. The CPT II activity of control fibroblasts was 0.28 ± 0.05 nmol/min/mg protein (n = 5), that of p.V368I (homozygous) was 0.27 ± 0.05 nmol/min/mg protein (n = 5), p.F352C (homozygous) was 0.18 ± 0.05 nmol/min/mg protein (n = 5), and p.F352C + p.V368I was 0.15 ± 0.05 nmol/min/mg protein (n = 5) (S2 Table). These results are similar to those reported in a previous study [20–23].

We previously reported that CPT II deficiency is a thermolabile phenotype of compound hetero-/homozygous variants [20–23], so we next evaluated the temperature sensitivity of CPT II variants. Fibroblast lysates were pre-incubated at 41°C or 30°C for 0–2 h, and then CPT II activities were measured at 30°C following the addition of L-carnitine and palmitoyl-CoA substrates (Fig. 1). Of the three variants, p.F352C + p.V368I was the most unstable, with significantly reduced enzyme activities during incubation at 41°C; under the same conditions, the activities of control fibroblasts and those from variants p.V368I (heterozygous) and p.V368I (homozygous) remained low and were also markedly reduced.

CPT II expression and dominant—negative effect

Previous studies of enzyme activity in fibroblasts of CPT II-deficient patients revealed similar CPT II activities for homozygous and compound heterozygous *CPT2* mutations [19], suggesting that mutant *CPT2* exert a dominant negative effect on the CPT II protein [31]. We therefore further examined the V_{max} and K_m values for L-carnitine of CPT II variant fibroblasts. V_{max} and K_m values of p.V368I (homozygous) were similar to those of p.F352C (heterozygous) + p.V368I (homozygous) (Fig. 2B). These data confirm an effect of homozygous and heterozygous *CPT2* mutations on the enzymatic properties of the homotetrameric protein compared with those of control CPT II.

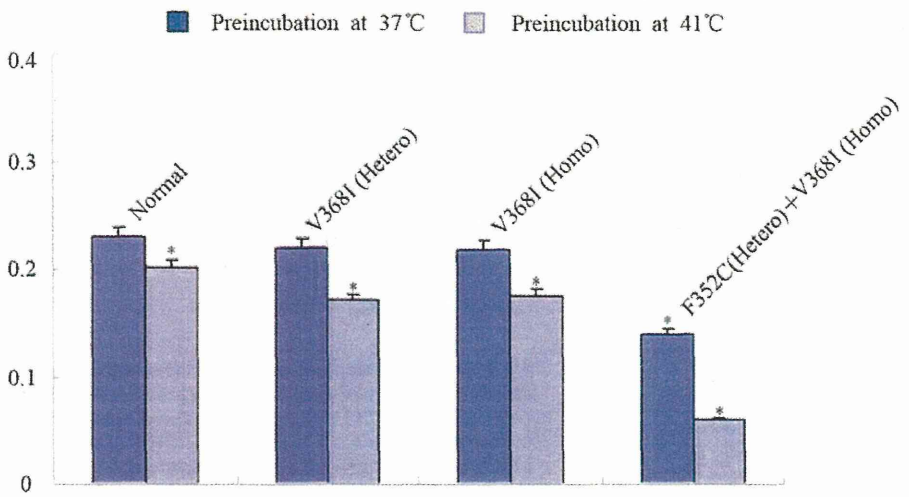

Fig 1. CPT II activities and thermal instability in CPT II-deficient fibroblasts. Fibroblast lysates were preincubated at 37°C or 41°C. Enzymatic reactions commenced by the addition of substrates at 37°C. Data are the means of five separate experiments. The average of three independent experiments is shown ± SEM (*P<0.05).

doi:10.1371/journal.pone.0119936.g001

To evaluate the stability of these variant CPT IIs, we analyzed CPT II mRNA and protein expression in control and patient fibroblasts. CPT II protein expression levels of p.F352C + p.V368I were significantly lower than p.V368I and p.V368I compared the CPT II protein expression levels of p.F352C +p.V368I with p.V368I and p.V368I according to Western Blotting (Fig. 2A, 2C), although mRNA levels, as measured by real-time PCR, were comparable (Fig. 2D). This indicates that the functional disorder of CPT II deficiency does not compromise the synthesis of polypeptides, but instead appears to impair the intracellular stability of folded CPT II proteins.

Short half-lives of CPT II variants

To examine the intracellular stability of CPT II variants, we metabolically labeled control and patient fibroblasts with L-[^{35}S] methionine and measured their half-lives using a pulse-chase protocol (Fig. 3, left). No differences were detected in the concentrations of newly synthesized and labeled CPT II proteins between the immunoprecipitates of control and patient fibroblasts, suggesting that the synthesis of control and patient CPT IIs was similarly efficient. Time course experiments showed that control CPT IIs had the longest half-life ($T^{1/2}$ ~ 18 h), similar to our

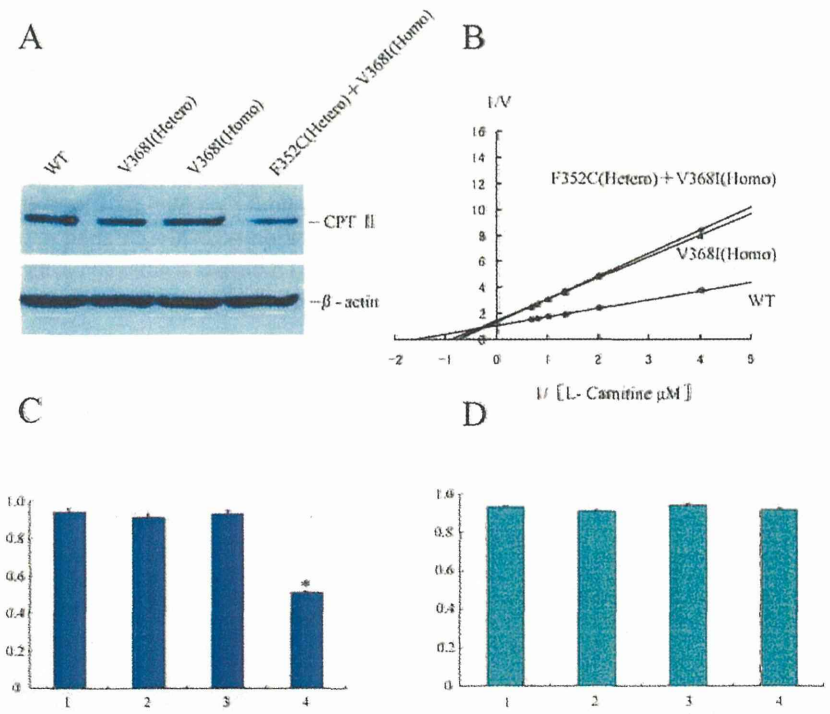

Fig 2. CPT II expression and the dominant—negative effect of *CPT II* variants on substrate-dependent kinetics. (A) CPT II expression was analyzed by Western Blotting with an anti-CPT II antibody. (B) Dominant—negative effect of *CPT II* variants was analyzed by substrate-dependent kinetics. (C) Relative protein expression of control and variant CPT II. (D) Real-time PCR analysis of control and variant *CPT II* expression. Lane 1, control fibroblasts; lane 2, V368I (heterozygous); lane 3, V368I (homozygous); lane 4, F352C (heterozygous) + V368I (homozygous). CPT II protein was expressed relative to β-actin. V_{max} and K_m values were obtained from kinetic analysis (1/*V* versus 1/[S] plots) by varying the concentrations of L-[methyl-^{3}H] carnitine between 0–300 μM at a fixed 50 μM palmitoyl-CoA concentration. (●) control, (▲) V368I (Homo), (◆) F352C (Hetero) + V368I (Homo). Data are means of three separate experiments. The average of three independent experiments is shown ± SEM (*P<0.05)

doi:10.1371/journal.pone.0119936.g002

previous data, while the half-life of p.V368I (homozygous) was shorter at $T^{1/2}$ ~ 10 h, and that of p.F352C (heterozygous) + p.V368I (homozygous) was significantly shorter, at $T^{1/2}$ ~ 4 h (Fig. 3, right).

Reduction of mitochondrial membrane potential

We assessed the mitochondrial membrane potential ($\Delta\Psi_m$) using the cationic lipophilic probe JC-1. Normal mitochondria with a high $\Delta\Psi_m$ appear red following aggregation of JC-1, which emits red fluorescence at ~590 nm. Following mitochondrial depolarization with a low $\Delta\Psi_m$, the JC-1 dye remains in its monomeric form, thereby emitting relatively more green (~525 nm) fluorescence [32]. We observed an increase of green fluorescence and a reduction of red fluorescence in the mitochondria of fibroblasts from patients with p.V368I (homozygous) and p.F352C (heterozygous) + p.V368I (homozygous) variants compared with mitochondria from control fibroblasts at both 37°C (Fig. 4A, B, C) and 41°C (Fig. 4D, E, F). Mitochondrial depolarization is a marker of mitochondrial dysfunction and precedes ATP depletion, so the data indicate a relatively low $\Delta\Psi_m$ of patient fibroblasts at 37°C and an enhanced decrease in $\Delta\Psi_m$ under heat-stress conditions at 41°C.

Cell apoptosis of CPT II variants

To assay cell apoptosis induced by CPT II deficiency, the percentage of apoptotic fibroblasts was measured in control and patient fibroblasts. Flow cytometry analysis revealed a significant increase in apoptosis of cultured patient fibroblasts from p.V368I (homozygous) and p.F352C (heterozygous) + p.V368I (homozygous) variants compared with control fibroblasts (Fig. 5A).

LDH is a stable cytoplasmic enzyme that catalyzes the interconversion of lactate and pyruvate. It is ubiquitously expressed in all cells and is rapidly released into the supernatant upon the plasma membrane damage. Therefore, measurement of its activity can be used to quantify plasma membrane damage. We observed a significant increase, seen as a percentage of LDH

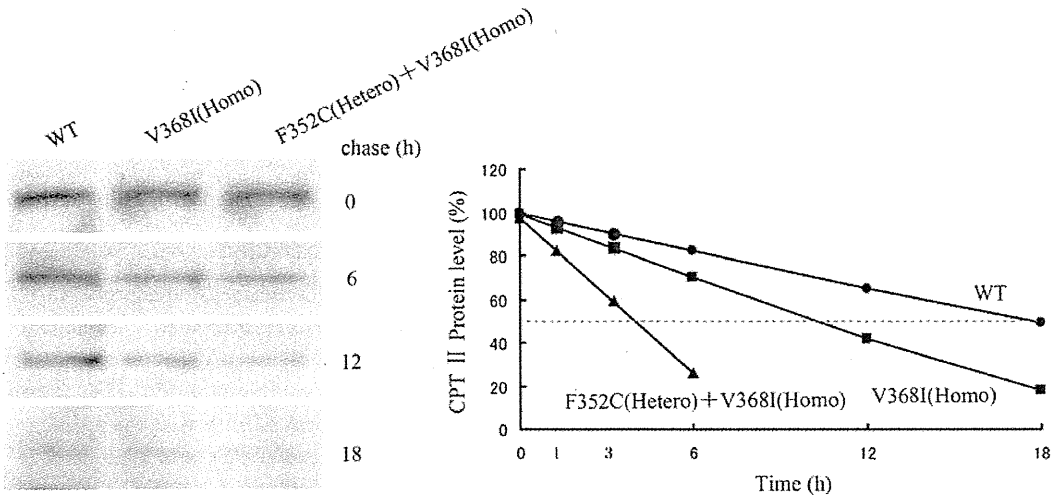

Fig 3. Pulse-chase (left) and half-lives (right) of control and variant CPT II in fibroblasts. Cultured fibroblasts were pulse-labeled with L-[^{35}S] methionine for 2 h and chased for 0, 6, 12, and 18 h. CPT II from fibroblast lysates was immunoprecipitated with anti-CPT II antibodies, then subjected to SDS-PAGE followed by autoradiography. (•) control, (□) V368I (homozygous), (▲) F352C (heterozygous) + V368I (homozygous). The average of three independent experiments is shown ± SEM.

doi:10.1371/journal.pone.0119936.g003

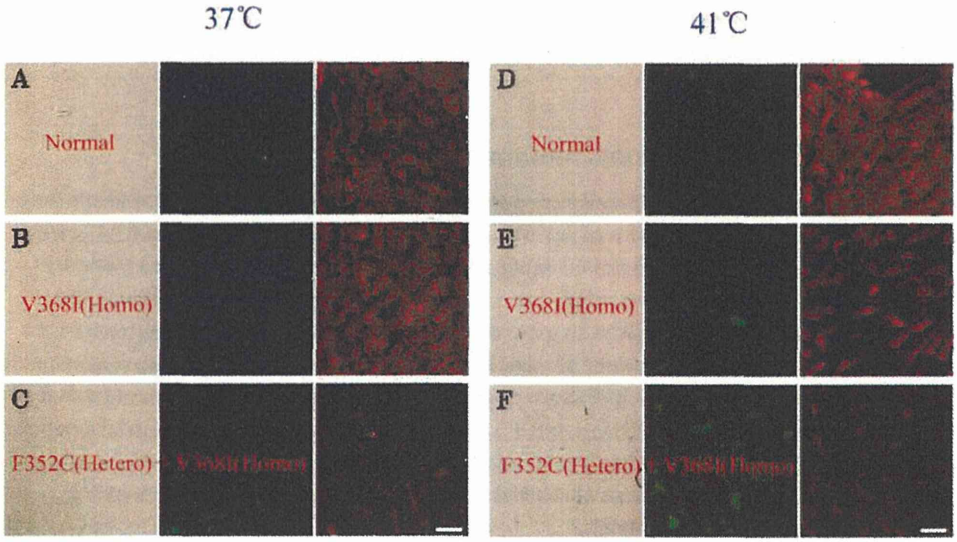

Fig 4. Reduction of mitochondrial membrane potential of control and variant CPT IIs in cultured fibroblasts. Control (A, D), V368I (homozygous) (B, E), and F352C (heterozygous) + V368I (homozygous) (C, F) fibroblasts were cultured at 37°C and 41°C. Mitochondrial depolarization was monitored by 15 min treatment with 10 μM of JC-1 in the dark and visualized under a fluorescence microscope. Scale bars, 100 μm.

doi:10.1371/journal.pone.0119936.g004

release, in damage to cultured patient fibroblasts p.V368I (homozygous) and p.F352C (heterozygous) + p.V368I (homozygous) (Fig. 5B).

To further evaluate the apoptotic effect in CPT II variants, the expression of apoptosis factors was analyzed by immunoblotting. Caspases are responsible for the deliberate of cells into apoptotic bodies during cell apoptosis. Caspases 3 and caspases 8 are situated at important junctions in apoptosis pathways, and activate disassembly in response to agents or insults that trigger the cytochrome c release from mitochondria. Caspase 3 amplifies caspase 8 initiation signals into a commitment to disassembly, while caspase 8 activates caspase 3 by proteolytic cleavage and cleaves vital cellular proteins. In the present study, Western Blotting showed that apoptotic factor was significantly released (Fig. 5C). Moreover, caspase-3, caspase-8, cytochrome c, and Bid, which induces apoptosis and allows the release of cytochrome c, were all expressed at higher levels in fibroblasts from p.V368I (homozygous) and p.F352C (heterozygous) + p.V368I (homozygous) variants compared with control fibroblasts.

Correlation between CPT II activity and ATP generation

To further clarify the metabolic disorder resulting from CPT II deficiency, the effects of thermal instability, CPT II enzymatic activities (S2 Table), fatty acid oxidation flux, and cellular ATP production were analyzed at 37°C and 41°C in patient fibroblasts p.V368I (homozygous), p.F352C (heterozygous) + p.V368I (homozygous) and control fibroblasts (Fig. 6). CPT II activities, ATP production, fatty acid oxidation and of fibroblasts from patients with the p.V368I (homozygous) variant were decreased to 85–95% of control values at 41°C and to 85–95% of control fibroblasts at 37°C. However, fibroblasts from patients with the p.F352C (heterozygous) + p.V368I (homozygous) variant exhibited significantly decreased CPT II activity to 40–60%, and ATP production and fatty acid oxidation to 50–70% of control values at 41°C, and to control fibroblasts at 37°C, with further inactivation of CPT II activity at increasing temperatures. The effect of the attenuated CPT II activity on cellular production of ATP was slightly less than that on fatty acid oxidation.

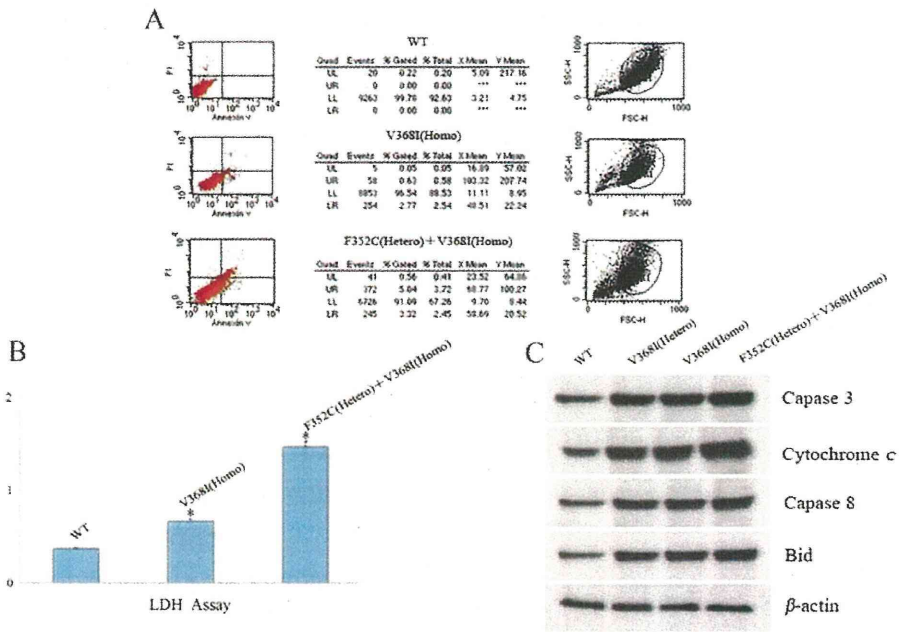

Fig 5. Cell apoptosis analysis of *CPT II* variants in fibroblasts. (A) Apoptotic fibroblasts were measured by flow cytometry. Fibroblasts incubated with DMSO were used as a control. (B) LDH assay of control and *CPT II* variants in fibroblasts. (C) Apoptotic factor release was analyzed by Western Blotting with antibodies against caspase-3, caspase-8, cytochrome c, and Bid for control and variant CPT IIs in control and CPT II-deficient fibroblasts. CPT II proteins are expressed relative to β-actin. Data are means of three separate experiments. The average of three independent experiments is shown ± SEM (*P<0.05).

doi:10.1371/journal.pone.0119936.g005

Discussion

Carnitine palmitoyltransferase II deficiency is the most common inborn errors of long-chain fatty acid oxidation and ATP generation, involving an increase in the concentrations of acylcarnitine in the serum [31–34]. In our previous data, we observed a transient and rapid increase of acylcarnitine ratio $[(C_{16:0} + C_{18:1})/C_2]$ to >0.09 in the serum during febrile convulsions that in the patients presenting with high risk influenza-associated encephalopathy, in the absence of previous episodes [24]. Because of the CPT II inactivation the rise in serum acylcarnitine probably caused by the presence of some disease causing mutations. However, these are not identical to the *CPT2* mutations observed in CPT II deficiency, which has a more severe phenotype.

Although a large proportion of CPT II deficiency patients exhibit phenotype of compound hetero/homozygous variations [26–30], the molecular mechanism of how the CPT II deficiency induces energy crisis has yet to be clarified. The genotype-phenotype correlation analysis of *CPT2* missense mutations has enabled the myopathic form of CPT II deficiency to be associated with "mild" mutations, while the null mutations resulting to truncation of mRNA or protein degradation are associated with the lethal neonatal forms [18, 30, 35–38]. Many disease causing mutations from inherited disorders effect on impair protein folding or reduce protein stability despite almost normal protein folding. In the present study, we analyzed three types of CPT II variations: p.V368I (heterozygous), p.V368I (homozygous), and p.F352C (heterozygous) + p.V368I (homozygous). Our data indicated that the fibroblasts of patients with these variants exhibited decreased enzyme activities, cellular β-oxidation, ATP generation, and $\Delta\Psi_m$, with increased *Km* values for L-carnitine, thermal instability, short half-lives, and cellular apoptosis. p.F352C (heterozygous) + p.V368I (homozygous) fibroblasts showed a particularly prominent

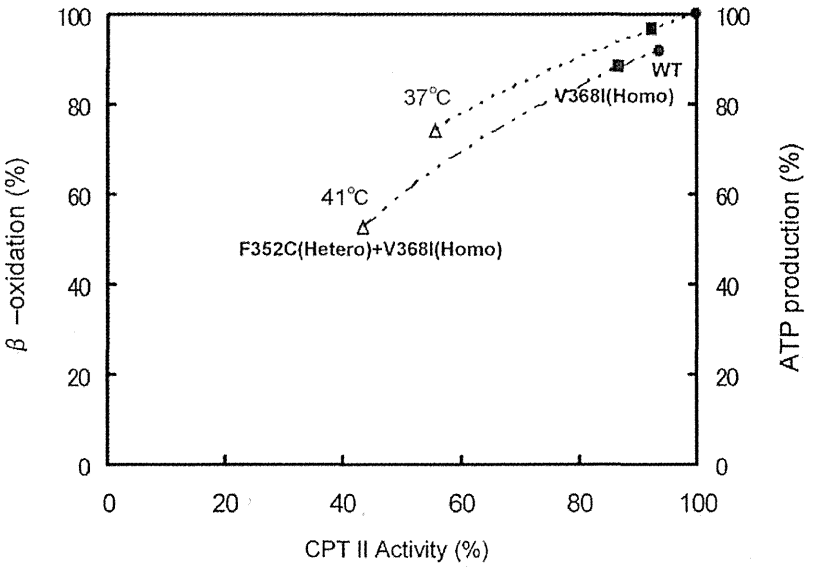

Fig 6. Correlation between CPT II activity and β-oxidation/ATP production at 41°C and 37°C in CPT II-deficient fibroblasts. (•) control, (□) V368I (homozygous), (△) F352C (heterozygous) + V368I (homozygous). CPT II activity, β-oxidation, and ATP production are expressed as % of control values of control fibroblasts at 37°C. Data areand means of five separate experiments: 0.53 nmol/min/mg protein of CPT II activity; 14.5 nmol of released CO_2/h/10^6 cells; 8.12 nmol of ATP/10^6 cells. The average of three independent experiments is shown ± SEM.

doi:10.1371/journal.pone.0119936.g006

decrease in enzyme activity, β-oxidation, ATP generation, $\Delta\Psi_m$, and lowered thermal stability, especially at 41°C and despite being located far from the acylcarnitine binding sites in the case of the p.F352C variant. The p.V368I variant is located near the acylcarnitine binding sites, though this appeared to have little effect on enzyme properties. Our work confirmed that CPT II variations have a dominant-negative effect on CPT II protein as shown previously in correlation researches between clinical metabolic and genotype data [18–26].

CPT2 mutations have been reported to cause several metabolic disorders including general muscle damage, temperature changes, infections, disturbances of Na^+/K^+ ATPases, neuroleptic syndrome, excessive use of muscular force, and conditions related to lipid metabolism increases. Patients with these disorders require more energy than that is provided by glycolytic system, so rely on that provided by fatty acid oxidation pathway. Because CPT II is not a rate limiting enzyme for fatty acid β-oxidation and ATP product, the activity decrease does not correlate linearly with the fatty acid β-oxidation or ATP generation decrease. However, the thermolabile phenotype of *CPT2* polymorphism p.F352C demonstrates reduced CPT II enzyme activity.

Our current study characterized the enzymatic properties of CPT II variants found in patients with CPT II deficiency and defined the correlation between genotype and metabolism of β-oxidation, ATP production, and ΔΨm. The p.F352C (heterozygous) + p.V368I (homozygous) variant is associated with an energy crisis, especially at high temperature, and as such is suspected to be a risk factor for acute encephalopathy. The sudden-onset brain edema with clinical manifestation in patients supports the ATP threshold hypothesis in the etiology of this kind edema. The significantly reduced ATP levels and markedly reduced ΔΨm observed in the fibroblasts of this variant at 41°C suggests that such thermolabile compound variants of CPT II reduced fuel utilization in brain endothelial cells may be a cause of this kind acute brain edema during fever in the affected patients [39–41]. Moreover, the short half-lives and thermal

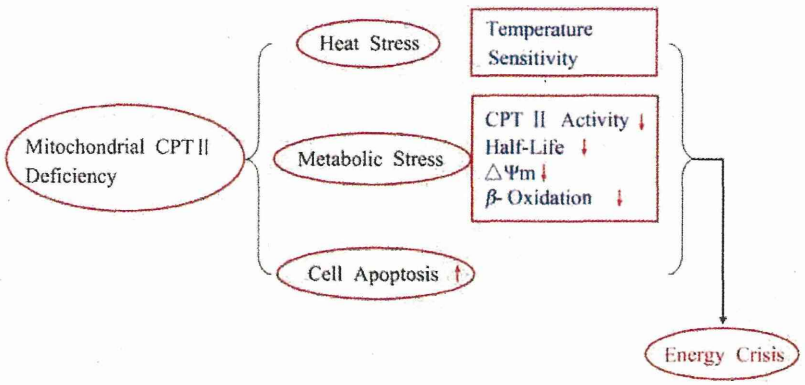

Fig 7. A proposed energy crisis pathway induced by CPT II deficiency.

doi:10.1371/journal.pone.0119936.g007

instability of these CPT II variants may play an important role in decreasing ATP levels below the phenotypic threshold. These acquired short half lives, cell apoptosis, impaired mitochondrial fuel utilization, together with the serum acylcarnitine level rise that occurs during high fever, could be hypothesized as the main cause of energy crisis and multiple organ failure (Fig. 7).

Fibrates are hypolipidemic drugs that increase lipoprotein levels by up-regulating the mRNA expression of metabolism genes via the steroid—thyroid PPARa transcription factor interactions. Bezafibrate has been reported to increase *CPT2* mRNA expression and to normalize enzyme activity in cultured CPT II-deficient fibroblasts. CPT II-deficient patients administered bezafibrate also showed a normalization of fatty acid oxidation levels, and increased CPT II mRNA and protein levels [42–44]. Additional studies are currently underway to further examine the effects of fibrates on CPT II-deficient patients.

Supporting Information

S1 Table. Primers used for CPT2 variants sequence analysis.
(DOC)

S2 Table. Enzymatic properties of normal and patient CPT IIs.
(DOC)

Acknowledgments

We greatly appreciate the editorial assistance of Ian Haigler.

Author Contributions

Conceived and designed the experiments: Dengbing Yao. Performed the experiments: MY MC YL XX. Analyzed the data: RY YZ. Contributed reagents/materials/analysis tools: Dengfu Yao YL. Wrote the paper: HK Dengbing Yao.

References

1. Bieber LL. Carnitine. Annu Rev Biochem. 1988; 57: 261–283. PMID: 3052273

2. Bonnefont JP, Demaugre F, Prip-Buus C, Saudubray JM, Brivet M, Abadi N, et al. Carnitine palmitoyltransferase deficiencies. Mol Genet Metab. 1999; 68: 424–440. PMID: 10607472

3. Bonnefont JP, Djouadi F, Prip-Buus C, Gobin S, Munnich A, Bastin J, et al. Carnitine palmitoyltransferases 1 and 2: biochemical, molecular and medical aspects. Mol Aspects Med. 2009; 25: 495–520.

4. Lehmann D, Zierz S. Normal protein content but abnormally inhibited enzyme activity in muscle carnitine palmitoyltransferase II deficiency, J Neurol Sci. 2014; 339(1–2):183–188. doi: 10.1016/j.jns.2014.01.033 PMID: 24656600

5. McGarry JD, Foster DW. Systemic carnitine deficiency. N Engl J Med. 1980; 303: 1413–1415. PMID: 7432389

6. McGarry JD, Mills SE, Long CS, Foster DW. Observations on the affinity for carnitine, and malonyl-CoA sensitivity, of carnitine palmitoyltransferase I in animal and human tissues. Demonstration of the presence of malonyl-CoA in non-hepatic tissues of the rat. Biochem J. 1983; 214: 21–28. PMID: 6615466

7. Pacilli A, Calienni M, Margarucci S, D'Apolito M, Petillo O, Rocchi L, et al. Carnitine-acyltransferase system inhibition, cancer cell death, and prevention of myc-induced lymphomagenesis. J Natl Cancer Inst. 2013; 105(7): 489–498. doi: 10.1093/jnci/djt030 PMID: 23486551

8. Murthy MS, Pande SV. Some differences in the properties of carnitine palmitoyltransferase activities of the mitochondrial outer and inner membranes. Biochem J. 1987; 248: 727–733. PMID: 3435481

9. Ronnett GV, Kim EK, Landree LE, Tu Y. Fatty acid metabolism as a target for obesity treatment. Physiol Behav. 2005; 85: 25–35. PMID: 15878185

10. Demaugre F, Bonnefont JP, Colonna M, Cepanec C, Leroux JP, Saudubray JM, et al. Infantile form of carnitine palmitoyltransferase II deficiency with hepatomuscular symptoms and sudden death. Physiopathological approach to carnitine palmitoyltransferase II deficiencies. J Clin Invest. 1991; 87: 859–864. PMID: 1999498

11. DiMauro S, DiMauro PM. Muscle carnitine palmityltransferase deficiency and myoglobinuria. Science. 1973; 182: 929–931. PMID: 4745596

12. Hug G, Bove KE, Soukup S. Lethal neonatal multiorgan deficiency of carnitine palmitoyltransferase II. N Engl J Med. 1991; 325: 1862–1864. PMID: 1961225

13. Taroni F, Verderio E, Fiorucci S, Cavadini P, Finocchiaro G, Uziel G, et al. Molecular characterization of inherited carnitine palmitoyltransferase II deficiency. Proc Natl Acad Sci USA. 1992; 89: 8429–8433. PMID: 1528846

14. Zierz S. Limited trypsin proteolysis renders carnitine palmitoyltransferase insensitive to inhibition by malonyl-CoA in patients with muscle carnitine palmitoyltransferase deficiency. Clin Invest. 1994; 72: 957–960.

15. Delorme L, Middleton PJ. Influenza A virus associated with acute encephalopathy. Am J Dis Child. 1979; 133: 822–824. PMID: 223436

16. Fujimoto S, Kobayashi M, Uemura O, Iwasa M, Ando T, Katoh T, et al. PCR on cerebrospinal fluid to show influenza-associated acute encephalopathy or encephalitis. Lancet. 1998; 352: 873–875. PMID: 9742980

17. Kasai T, Togashi T, Morishima T. Encephalopathy associated with influenza epidemics. Lancet. 2000; 355(9214):1558–1559. PMID: 10801205

18. Olpin SE, Afifi A, Clark S, Manning NJ, Bonham JR, Dalton A, et al. Mutation and biochemical analysis in carnitine palmitoyltransferase type II (CPT II) deficiency. J Inherit Metab Dis. 2003; 26: 543–557. PMID: 14605500

19. Thuillier L, Rostane H, Droin V, Demaugre F, Brivet M, Kadhom N, et al. Correlation between genotype, metabolic data, and clinical presentation in carnitine palmitoyltransferase 2 (CPT2) deficiency. Hum Mutat. 2003; 21: 493–501. PMID: 12673791

20. Yao D, Mizuguchi H, Yamaguchi M, Yamada H, Chida J, Shikata K, et al. Thermal instability of compound variants of carnitine palmitoyltransferase II and impaired mitochondrial fuel utilization in influenza-associated encephalopathy. Hum Mutat. 2008; 29(5): 718–727. doi: 10.1002/humu.20717 PMID: 18306170

21. Yao M, Yao D, Yamaguchi M, Chida J, Yao D, Kido H. Bezafibrate upregulates carnitine palmitoyltransferase II expression and promotes mitochondrial energy crisis dissipation in fibroblasts of patients with influenza-associated encephalopathy. Mol Genet Metab. 2011; 104(3): 265–272. doi: 10.1016/j.ymgme.2011.07.009 PMID: 21816645

22. Yao D, Yao M, Yamaguchi M, Chida J, Kido H. Characterization of compound missense mutation and deletion of carnitine palmitoyltransferase II in a patient with adenovirus-associated encephalopathy. J Med Invest. 2011; 58(3–4): 210–218. PMID: 21921426

23. Chen Y, Mizuguchi H, Yao D, Ide M, Kuroda Y, Shigematsu Y, et al. Thermolabile phenotype of carnitine palmitoyltransferase II variations as a predisposing factor for influenza-associated encephalopathy. FEBS Lett. 2005; 579: 2040–2044. PMID: 15811315

24. Saudubray JM, Coude FX, Demaugre F, Johnson C, Gibson KM, Nyhan WL. Oxidation of fatty acids in cultured fibroblasts: a model system for the detection and study of defects in oxidation. Pediatr Res. 1982; 16: 877–881. PMID: 7145511

25. Isackson PJ, Bennett MJ, Vladutiu GD. Identification of 16 new disease-causing mutations in the CPT2 gene resulting in carnitine palmitoyltransferase II deficiency. Mol Genet Metab. 2006; 89: 323–331. PMID: 16996287

26. Rufer AC, Thoma R, Benz J, Stihle M, Gsell B, De Roo E, et al. The crystal structure of carnitine palmitoyltransferase 2 and implications for diabetes treatment. Structure. 2006; 14: 713–723. PMID: 16615913

27. Taggart RT, Smail D, Apolito C, Vladutiu GD. Novel mutations associated with carnitine palmitoyltransferase II deficiency. Hum Mutat. 1999; 13: 210–220. PMID: 10090476

28. Verderio E, Cavadini P, Montermini L, Wang H, Lamantea E, Finocchiaro G, et al. Carnitine palmitoyltransferase II deficiency: structure of the gene and characterization of two novel disease-causing mutations. Hum Mol Genet. 1995; 4: 19–29. PMID: 7711730

29. Weiser M, Frishman WH, Michaelson MD, Abdeen MA. The pharmacologic approach to the treatment of obesity. J Clin Pharmacol. 1997; 37: 453–473. PMID: 9208352

30. Yahyaoui R, Espinosa MG, Gómez C, Dayaldasani A, Rueda I, Roldán A, et al. Neonatal carnitine palmitoyltransferase II deficiency associated with Dandy-Walker syndrome and sudden death. Mol Genet Metab. 2011; 104(3): 414–416. doi: 10.1016/j.ymgme.2011.05.003 PMID: 21641254

31. Wataya K, Akanuma J, Cavadini P, Aoki Y, Kure S, Invernizzi F, et al. Two CPT2 mutations in three Japanese patients with carnitine palmitoyltransferase II deficiency: functional analysis and association with polymorphic haplotypes and two clinical phenotypes. Hum Mutat. 1998; 11: 377–386. PMID: 9600456

32. Ørngreen MC, Dunø M, Ejstrup R, Christensen E, Schwartz M, Sacchetti M, et al. Fuel utilization in subjects with carnitine palmitoyltransferase 2 gene mutations. Ann Neurol. 2005; 57: 60–66. PMID: 15622536

33. Lee S, Jeong SY, Lim WC, Kim S, Park YY, Sun X, et al. Mitochondrial Fission and Fusion Mediators, hFis1 and OPA1, Modulate Cellular Senescence. J Biol Chem. 2007; 282: 22977–22983. PMID: 17545159

34. Tamaoki Y, Kimura M, Hasegawa Y, Iga M, Inoue M, Yamaguchi S, et al. A survey of Japanese patients with mitochondrial fatty acid beta-oxidation and related disorders as detected from 1985 to 2000. Brain Dev. 2002; 24: 675–680. PMID: 12427513

35. Kobayashi Y, Ishikawa N, Tsumura M, Fujii Y, Okada S, Shigematsu Y, et al. Acute severe encephalopathy related to human herpesvirus-6 infection in a patient with carnitine palmitoyltransferase 2 deficiency carrying thermolabile variants. Brain Dev. 2013; 35(5): 449–453. doi: 10.1016/j.braindev.2012.06.013 PMID: 22854105

36. Fanin M, Anichini A, Cassandrini D, Fiorillo C, Scapolan S, Minetti C, et al. Allelic and phenotypic heterogeneity in 49 Italian patients with the muscle form of CPT-II deficiency. Clin Genet. 2012; 82(3): 232–239. doi: 10.1111/j.1399-0004.2011.01786.x PMID: 21913903

37. Anichini A, Fanin M, Vianey-Saban C, Cassandrini D, Fiorillo C, Bruno C, et al. Genotype-phenotype correlations in a large series of patients with muscle type CPT II deficiency. Neurol Res. 2011; 33 (1):24–32. doi: 10.1179/016164110X12767786356390 PMID: 20810031

38. Sigauke E, Rakheja D, Kitson K, Bennett MJ. Carnitine palmitoyltransferase II deficiency: a clinical, biochemical, and molecular review. Lab Invest. 2003; 83(11):1543–1454. PMID: 14615409

39. Tahanian E, Peiro S, Annabi B. Low intracellular ATP levels exacerbate carcinogen-induced inflammatory stress response and inhibit in vitro tubulogenesis in human brain endothelial cells. J Inflamm Res. 2011; 4:1–10. doi: 10.2147/JIR.S15880 PMID: 22096365

40. Manda KR, Banerjee A, Banks WA, Ercal N. Highly active antiretroviral therapy drug combination induces oxidative stress and mitochondrial dysfunction in immortalized human blood-brain barrier endothelial cells. Free Radic Biol Med. 2011; 50(7): 801–810. doi: 10.1016/j.freeradbiomed.2010.12.029 PMID: 21193030

41. Anwar Z, Albert JL, Gubby SE, Boyle JP, Roberts JA, Webb TE, et al. Regulation of cyclic AMP by extracellular ATP in cultured brain capillary endothelial cells. Br J Pharmacol. 1999; 128(2): 465–471. PMID: 10510459

42. Rossignol R, Malgat M, Mazat JP, Letellier T. Threshold effect and tissue specificity. Implication for mitochondrial cytopathies. J Biol Chem. 1999; 274: 33426–33432. PMID: 10559224

43. Wieser T. Carnitine Palmitoyltransferase II Deficiency, Synonym: CPT II Deficiency. Gene Reviews. 2011.

44. Angelini C, Semplicini C. Metabolic myopathies: the challenge of new treatments. Curr Opin Pharmacol. 2010; 10: 338–345. doi: 10.1016/j.coph.2010.02.006 PMID: 20356791

Am J Physiol Heart Circ Physiol 307: H922–H932, 2014.
First published July 18, 2014; doi:10.1152/ajpheart.00076.2014.

Ectopic trypsin in the myocardium promotes dilated cardiomyopathy after influenza A virus infection

Hai-Yan Pan,[1] Hua-Mei Sun,[1] Lu-Jing Xue,[1] Min Pan,[1] Yi-Ping Wang,[1] Hiroshi Kido,[2] and Jian-Hua Zhu[1]

[1]*Department of Cardiology, Affiliated Hospital of Nantong University, Institute of Cardiovascular Research, Nantong University, Jiangsu, China; and* [2]*Division of Enzyme Chemistry, Institute for Enzyme Research, The University of Tokushima, Tokushima, Japan*

Submitted 3 February 2014; accepted in final form 11 July 2014

Pan H, Sun H, Xue L, Pan M, Wang Y, Kido H, Zhu J. Ectopic trypsin in the myocardium promotes dilated cardiomyopathy after influenza A virus infection. *Am J Physiol Heart Circ Physiol* 307: H922–H932, 2014. First published July 18, 2014; doi:10.1152/ajpheart.00076.2014.—We have previously reported that ectopic trypsin in the myocardium triggers acute myocarditis after influenza A virus (IAV) infection. As myocarditis is a common precursor to dilated cardiomyopathy (DCM), the aim of the present study was to investigate the influence of trypsin on the progression of DCM after IAV infection. IAV-infected mice treated with saline or trypsin inhibitor were euthanized on *days 0, 9, 20, 40* and *60* postinfection. Trypsin expression colocalized with myocardial inflammatory loci and IAV-induced myocarditis peaked on *day 9* postinfection and alleviated by *day 20* but persisted until *day 60* postinfection, even though replication of IAV was not detected from *day 20* postinfection. Similar time courses were observed for the activation of pro-matrix metalloproteinase (pro-MMP)-9 and expression of the proinflammatory cytokines IL-6, IL-1β, and TNF-α. Degradation of collagen type I, proliferation of ventricular interstitial collagen, and expression of collagen type I and III mRNA increased significantly during acute and chronic phases; collagen type III mRNA increased more significantly than collagen type I mRNA. Cardiac function progressively deteriorated with progressive left ventricular dilation. The trypsin inhibitor aprotinin suppressed pro-MMP-9 activation and cytokine release, alleviated myocardial inflammation, and restored collagen metabolism during acute and chronic phases of myocarditis. This effectively prevented ventricular dilation and improved cardiac function. These results suggest that ectopic trypsin in the myocardium promoted DCM through chronic activation of pro-MMP-9, persistent induction of cytokines, and mediation of collagen remodeling. Pharmacological inhibition of trypsin activity might be a promising approach for the prevention of viral cardiomyopathy.

trypsin; myocarditis; dilated cardiomyopathy; influenza virus; extracellular matrix remodeling

THE INFLUENZA A VIRUS (IAV) is the most common infectious pathogen in humans. Acute myocarditis is a well-known complication of influenza infection and a common prelude to inflammatory dilated cardiomyopathy (DCM) that can lead to chronic heart failure (1, 49). A long-term followup study (18) in patients with acute myocarditis documented the development of DCM in 21% of patients over a mean followup period of 3 yr. The course of viral myocarditis has three distinct, successive stages: acute viral infection, immune cell infiltration, and cardiac remodeling (29). Although progress has been made in understanding the pathogenesis of DCM after viral infection, the precise mechanisms involved in the transition from viral myocarditis to DCM are not well understood.

During IAV infection, host factors such as proinflammatory cytokines, matrix metalloproteinases (MMPs), and ectopic trypsin are induced (39). Among these factors, ectopic trypsin, serving as a viral envelope hemagglutinin-processing protease, is crucial for viral entry, replication, and spread, because the IAV genome does not have a hemagglutinin-processing protease and hemagglutinin cleavage by cellular proteases at the posttranscriptional level is a prerequisite for membrane fusion activity (16). The expression profile of trypsin is likely a major determinant of IAV tissue tropism and pathogenicity. In addition, trypsin converts pro-MMPs to active MMPs (20, 39, 44) and promotes cytokine release through proteinase-activated receptor (PAR)-2 (35). Active MMPs, such as MMP-2 and MMP-9, degrade vascular basement membranes and the extracellular matrix (ECM), which could promote endothelial hyperpermeability and inflammatory cell migration (53). Degradation of the ECM could initiate anoikis in neighboring healthy tissue (31), leading to cardiac dilation and dysfunction. Furthermore, active MMP-2 and MMP-9 convert proinflammatory cytokines into their active forms (9, 28). Activated cytokines, such as TNF-α, IL-1β, and IL-6 recruit inflammatory cells and increase nitric oxide production in the heart (42) and promote cardiac remodeling via serpin A-3n (5). Overproduction of nitric oxide contributes to the development of DCM by inducing myocardial ATP depletion and cardiomyocyte apoptosis (14, 48).

The myocardial ECM is mainly composed of collagen type I (Col I; 85%) and Col type III (Col III; 11%) (8), which provide architectural support for cardiac myocytes and are important in myocardial function (41). Collagenases like MMP-9 and MMP-2 can remove collagen from struts and tethers, which are critical structures for preventing myocyte slippage (11, 23). Proinflammatory cytokines induce new collagen deposition, which can be misdirected to intercellular septa with a defective content of permanent cross-links (24). These effects can contribute to heart overextension and dilation.

We have previously reported that IAV-induced trypsin expression in the myocardium triggers acute viral myocarditis through stimulation of IAV replication, pro-MMP-9 activation, and cytokine induction (39). The aim of the present study was to clarify the role of trypsin in the progression of DCM after IAV infection. We defined the kinetics of trypsin upregulation during acute and chronic phases of myocarditis and investigated the effects of trypsin upregulation on the persistence of myocardial inflammation, changes in myocardial interstitial collagen components, and DCM development. The results

Address for reprint requests and other correspondence: J.-H. Zhu, Dept. of Cardiology, Affiliated Hospital of Nantong Univ., Institute of Cardiovascular Research, Nantong Univ., Jiangsu 226001, China (e-mail: dr.zhujianhua@gmail.com).

suggested that trypsin inhibition might prevent DCM with improved cardiac function after IAV infection.

METHODS

Influenza myocarditis model. This study conformed with Animal Research: Reporting In Vivo Experiments guidelines (17) and was approved by the Animal Care Committee of Nantong University. We randomly assigned 90 specific pathogen-free 8-wk-old male BALB/c mice (Comparative Medicine Center of Yangzhou University, Jiangsu, China) to a mock-infected group or to IAV-infected groups treated with saline or the trypsin inhibitor aprotinin (n = 10 mice/group). Under chloral hydrate anesthesia, mice were infected intranasally with 40 plaque-forming units of IAV/PR/8/34 (H1N1) (VR1469, American Type Culture Collection) in 15 μl saline or saline vehicle and euthanized on *days 0, 9, 20, 40,* or *60* postinfection. To analyze the effects of trypsin inhibition, aprotinin (Sigma-Aldrich Shanghai Trading, Shanghai, China) was injected intraperitoneally at 4 mg/kg daily until euthanasia.

Hemodynamic measurements. Transthoracic echocardiography was performed in mice using a VisualSonics vevo 770 ultrasonograph with a 30-MHz transducer (VisualSonics, Toronto, ON, Canada) under light anesthesia from an intramuscular injection of ketamine (30 mg/kg) before euthanasia. Left ventricular (LV) M-mode echocardiograms were obtained from a parasternal short-axis view. LV end-diastolic dimension (LVEDD), LV end-systolic dimension (LVESD), LV posterior wall thickness at end diastole (LVPWd), and LV posterior wall thickness at end systole (LVPWs) were recorded. Fractional shortening (FS) was calculated as follows: FS = (LVEDD − LVESD)/LVEDD × 100. LV end-diastolic volume (LVEDV) and LV end-systolic volume (LVESV) were measured from the parasternal long-axis view and calculated using Simpson's formula (4). Stroke volume (SV) and cardiac output (CO) were calculated by the following formulas: SV = LVEDV − LVESV and CO = SV × heart rate, respectively. LV ejection fraction (EF) was calculated as follows: EF = (SV/LVEDV) × 100. All parameters were measured from three consecutive cycles and averaged.

ELISA. Mouse blood was collected from the right ventricle after anesthesia. Plasma levels of Col I cross-linked carboxy-terminal telopeptide (ICTP) were measured with ELISA kits according to the recommendation of the manufacturer (Antibodies-online).

Tissue preparation. Isolated hearts were cut into halves with one portion fixed with 4% buffered paraformaldehyde solution for histopathological evaluation and the other portion stored at −80°C for biochemical analyses. All experiments were repeated at least three times.

Histopathological preparation. Tissues fixed in 4% paraformaldehyde were dehydrated in graded ethanol, embedded in paraffin, and sliced into 5-μm sections. After deparaffinization, sections were subjected to routine hematoxylin and eosin staining or van Gieson staining for the identification of collagen distribution.

Immunostaining. Immunohistochemistry for upregulated trypsin in the myocardium was performed as previously described (22, 39). Endogenous peroxidase activity was quenched with 3% H_2O_2 in methanol. Nonspecific binding sites were blocked with goat serum. Immune depositions in sections were detected with rabbit anti-trypsin antibody (Santa Cruz Biotechnology). Avidin-biotin-peroxidase kits (Vector Labs, Burlingame, CA) were used to visualize trypsin. For immunofluorescent staining, rabbit anti-trypsin (Santa Cruz Biotechnology) and mouse anti-IAV (Takara Bio, Shiga, Japan) were used as primary antibodies. Goat anti-rabbit IgG Texas red-conjugated antibody (Molecular Probes) and goat anti-mouse IgG FITC-conjugated antibody (Sigma-Aldrich) were used as secondary antibodies to visualize trypsin and IAV immunodeposits in hearts.

RT-PCR. Total RNA was extracted with TRIzol Reagent (Sangon Biotech, Shanghai, China), and 2 μg RNA was reverse transcribed with a TIANScript cDNA Synthesis kit (Tiangen Biotech, Beijing, China) for the synthesis of host and IAV cDNA. Trypsin, IAV nonstructural protein (NS)1, Col I, and Col III gene segments were amplified with a Taq PCR MasterMix kit (Tiangen Biotech) as previously described (15, 39). RT-PCR products were analyzed by agarose gel electrophoresis and visualized by treatment with ethidium bromide.

Immunoblot analysis and gelatin zymograph. Tissues were homogenized with three volumes of 0.05 M Tris·HCl (pH 7.6) containing 2% SDS and 0.5 M NaCl. Immunoblot analysis was performed as previously described (22). Target-specific antibodies were used to detect trypsin, MMP-9, MMP-2, TNF-α, IL-6, IL-1β, and actin (Santa Cruz Biotechnology). Immunoreactive bands were visualized by an enhanced chemiluminescence detection system (Cell Signaling Technology). MMP-2 and MMP-9 activities were analyzed by zymography. Protein extracts were separated by electrophoresis on 10% gelatin zymogram gels (Invitrogen) at 4°C. Gels were incubated in renaturing buffer (Invitrogen) at room temperature for 30 min and in developing buffer (Invitrogen) at 37°C for 4 h. Bands of gelatin degradation were visualized by staining with Coomassie brilliant blue R-250 and destaining as appropriate.

Morphometric quantification of trypsin and collagen. Digital images from immunohistochemistry and van Gieson staining were obtained using a Nikon E800 microscope with a ×10 objective lens (Nikon Instruments, Tokyo, Japan). Trypsin and collagen were quantified from 12 separate fields over 3 stained sections for each heart using Image Proplus software and expressed as percentages of the stained area per total myocardial tissue area.

Statistical analysis. Results are presented as means ± SD from 7–10 mice/group. Significance was calculated by one-way ANOVA. For survival analysis, the Gehan-Breslow-Wilcoxon test was used for the analysis of survival difference. P values of <0.05 were considered statistically significant.

RESULTS

Kinetics of body weight, survival rate, and myocardial inflammation as well as restoration by trypsin inhibitor. We have previously reported that the inflammatory response in the myocardium was most serious on *day 9* after viral infection (39). Biventricular dilation consistent with DCM was observed on *day 35* postinfection in male Balb/c mice and on *day 60* postinfection in male C3H/He mice (38, 46). Therefore, we observed the progression of myocardial inflammation from *day 9* to *60* postinfection. The severity of IAV infection was evaluated by weight loss, survival rate, and myocardial pathological changes. Mice intranasally inoculated with 40 plaque-forming units of IAV/PR/8 (H1N1) appeared lethargic and anorexic with significant weight loss in the acute stage ($P <$ 0.01; Fig. 1*A*). About 20–30% of mice died around *day 9* postinfection if not treated with aprotinin. No mice died after *day 20* postinfection (Fig. 1*B*). Surviving mice exhibited acute and chronic myocarditis, as confirmed by histological examination of hematoxylin and eosin-stained sections. Extensive inflammatory infiltration across the interstitium accompanied by focal necrosis and ECM destruction were observed on *day 9* in infected mice not treated with the trypsin inhibitor aprotinin. The prevalence of infiltration was alleviated by *day 20* postinfection but persisted with sparse, diffuse inflammatory cells in the interstitium on *day 60* postinfection (Fig. 1*C,1*). Aprotinin significantly reduced the loss of body weight, decreased morbidity, and suppressed the inflammatory response, which alleviated cardiac lesions (Fig. 1, *A*, *B*, and *C,2*).

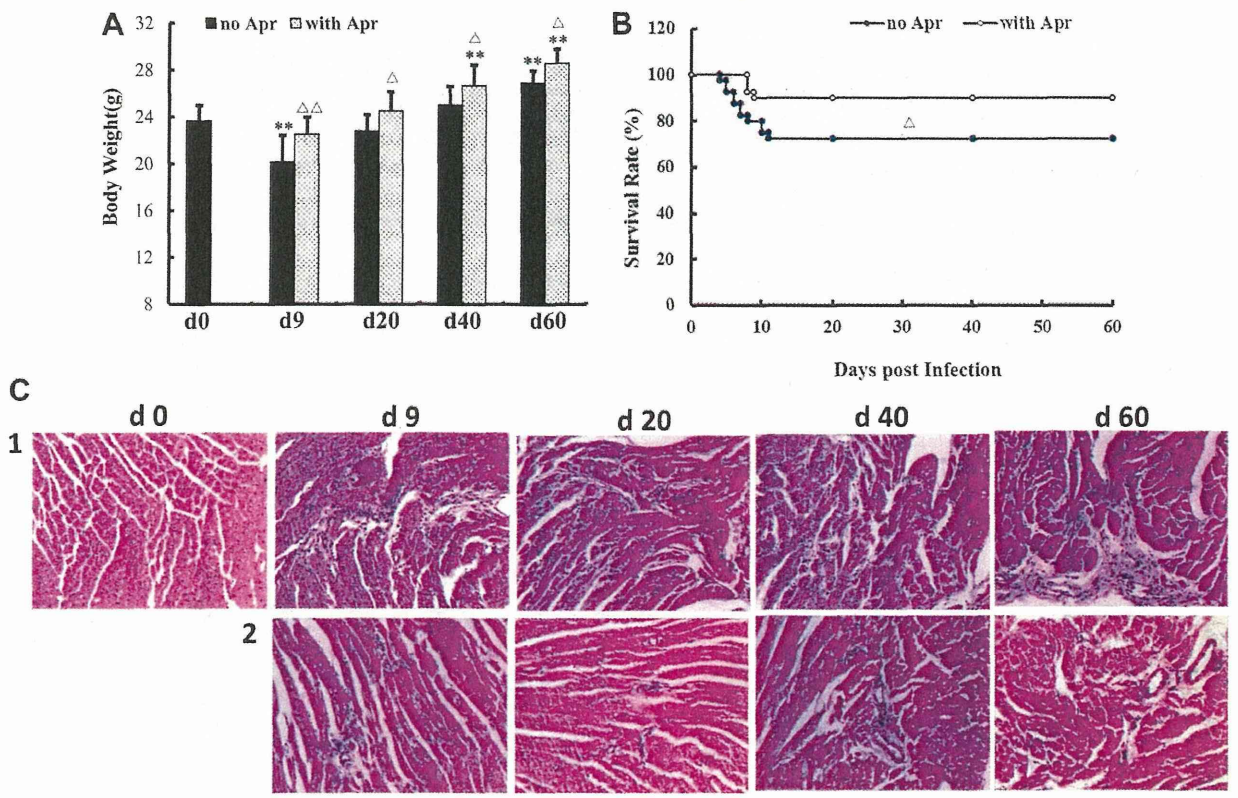

Fig. 1. Kinetics of body weight, survival rate, and myocardial inflammation. *A*: comparison of mouse body weights at different time points postinfection (n = 7–10 mice/group). $^{**}P < 0.01$ vs. *day* (d)*0*; $\triangle P < 0.05$ and $\triangle\triangle P < 0.01$ vs. no aprotinin (Apr) treatment at the same time point. *B*: Kaplan-Meier survival curve showing statistically significant differences in survival rates between mice treated with and without Apr (n = 40 mice with no Apr treatment and 40 mice with Apr treatment). $\triangle P < 0.05$ vs. no Apr treatment. *C*: myocardial inflammation monitored by hematoxylin and eosin staining from *days 0* to *60* postinfection without (*1*) and with (*2*) Apr treatment. Magnification: ×100.

Kinetics of viral replication and activation of trypsinogen with suppression by trypsin inhibitor. The kinetics of viral replication in hearts, as monitored by viral NS1 gene expression, showed that viral RNA peaked on *day 9* postinfection and then diminished to undetectable levels by *day 20* postinfection (Fig. 2*A*). Trypsin gene expression as monitored by RT-PCR and expression of trypsinogen plus trypsin and calculation of the trypsin-to-trypsinogen ratio based on Western blot analysis also peaked on *day 9* and then slowly declined to minimum levels by *day 60* postinfection, although levels were still higher than controls (*day 0*; Fig. 2, *A–D*). Immunofluorescent staining showed that trypsin distributed in the myocardium of infected loci during the acute stage. Immunohistochemical staining revealed that trypsin was mainly expressed by myocardial cells, which colocalized with inflammatory infiltrates (Fig. 2, *E* and *G*). The level of stained trypsin depositions quantified by area percentage was highest on *day 9* postinfection and declined gradually as myocardial inflammation declined during the chronic phase (*days 20* to *60* postinfection; Fig. 2*F*). Aprotinin significantly suppressed viral replication on *day 9* postinfection and inhibited upregulation of trypsin expression around inflammatory loci and the trypsin-to-trypsinogen ratio during both acute and chronic phases.

Kinetics of MMPs and cytokine upregulation by IAV and effects of trypsin inhibitor. The relationships among trypsin upregulation, MMP activation, and cytokine induction were analyzed in acute and chronic myocarditis. Along with an increase in trypsin levels, upregulated pro-MMP-9 was effectively converted to active MMP-9, although upregulated pro-MMP-2 was not activated (Fig. 3). MMP-9 activity, total MMP-9 (pro-MMP-9 plus active MMP-9) expression, and the active MMP-9-to-pro-MMP-9 ratio increased to a peak value on *day 9* postinfection followed by a slow decrease to *day 60* postinfection (Fig. 3). Similar induction time courses were observed for IL-6, IL-1β, and TNF-α (Fig. 4). Aprotinin significantly inhibited MMP-9 activity and suppressed upregulation of MMPs and activation of pro-MMP-9 as well as the induction of cytokines during acute and chronic myocarditis.

Increased Col I degradation in the myocardium was prevented by trypsin inhibitor. Both trypsin and MMP-9 efficiently degrade Col I (33, 37), and ICTP is released during hydrolysis of Col I fibrils. The amount of ICTP in the circulation is proportional to the amount of degraded fibrillar collagen (26). Therefore, ICTP was used as a marker for Col I degradation. Consistent with the observed changes in trypsin and MMP-9 expression, ICTP levels significantly increased on *day 9* postinfection and then slowly decreased from *day 20* postinfection, although on *day 60* postinfection levels did not match those in control mice. Aprotinin significantly decreased ICTP levels during acute and chronic phases, suggesting a prevention of Col I degradation (Fig. 5*A*).

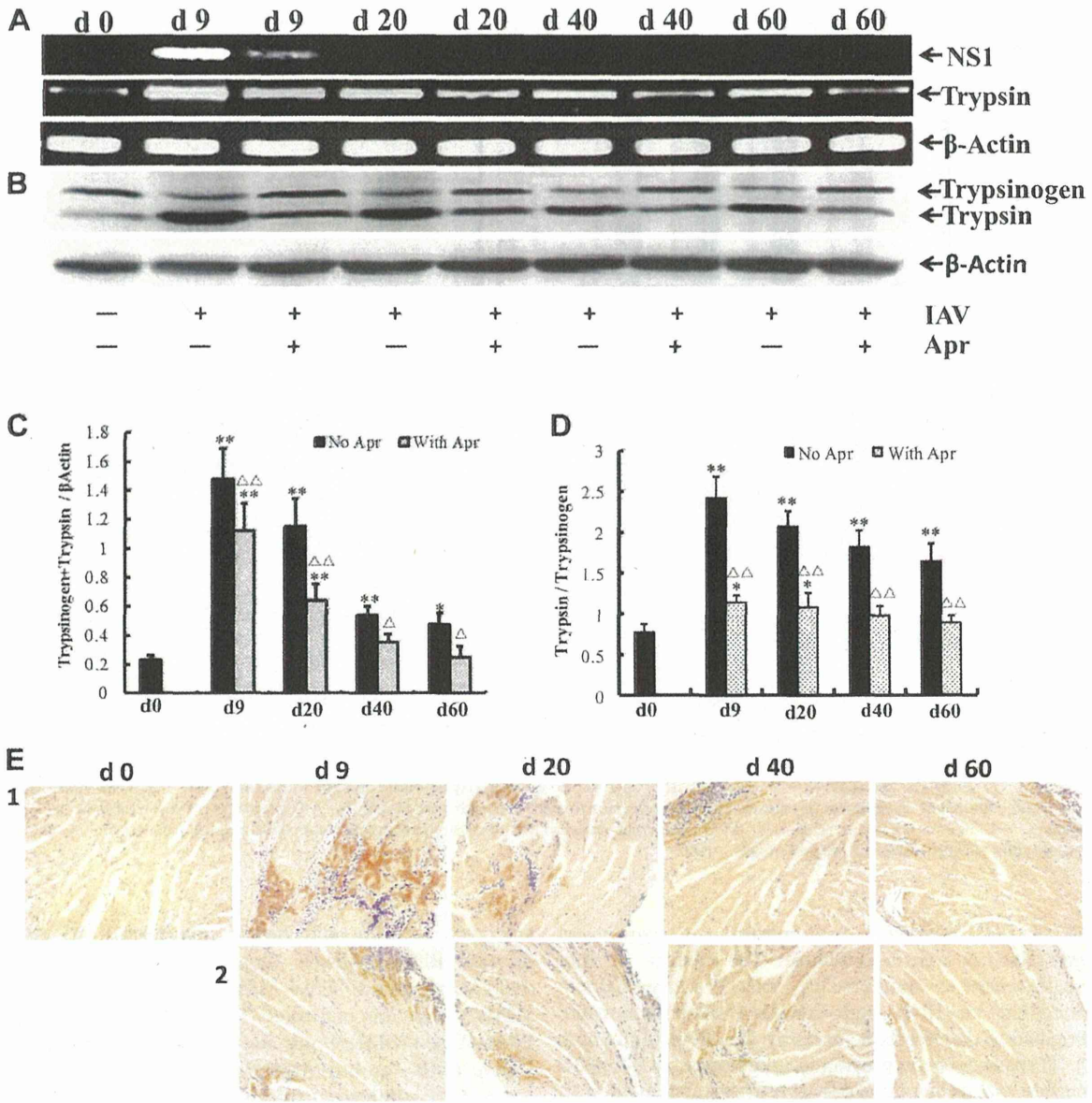

Fig. 2. Viral replication and activation of trypsinogen in the myocardium as well as colocalization of trypsin with inflammatory loci and influenza A virus (IAV). *A*: kinetics of viral nonstructural protein (NS)1 and trypsin gene expression by RT-PCR. *B*: expression of trypsinogen and trypsin by Western blot analysis. Band intensity was quantified by densitometry. β-Actin was the internal control. *C* and *D*: upregulation of trypsinogen + trypsin and activation of trypsinogen were significantly inhibited by Apr from *days 0* to *60* postinfection. Data are averages ± SD of 3 independent experiments from 7–10 mice/group. $^{*}P < 0.05$ and $^{**}P < 0.01$ vs. *day 0*; $\triangle P < 0.05$ and $\triangle\triangle P < 0.01$ vs. no Apr at the same observation time. *E*: immunohistochemical detection of upregulated trypsin in the myocardium without (*1*) and with (*2*) Apr treatment. *F*: quantified area percentage of trypsin ($n = 5$ mice/group). $^{**}P < 0.01$ vs. *day 0*; $\triangle\triangle P < 0.01$ vs. no Apr at the same observation time. *G*: representative immunofluorescent staining of IAV (green) and trypsin (red) in the myocardium without and with Apr treatment on *days 9* and *20* postinfection. Merged results are shown on the *right*. Magnification: ×100.

Increased collagen deposition in the myocardium reduced by trypsin inhibitor. During cardiac remodeling, loss of collagen from increased collagen degradation leads to replacement by newly synthesized collagen (21). To observe collagen proliferation and deposition after IAV infection, we used van Gieson staining. Heavy accumulation of collagen was seen around the blood vessels and inflammatory loci on *day 9* postinfection. From *day 20* postinfection, an extensive proliferation of collagen across the ventricular interstitium was observed and was most obvious on *day 60* postinfection. The increased collagen deposition was reduced in aprotinin-treated mice during acute and chronic phases (Fig. 5, *B* and *C*).

Increased Col I and Col III mRNA in the myocardium was suppressed by trypsin inhibitor. Cardiac ECM remodeling is associated with significant changes in Col I and Col III expression (45). Synthesis of Col I and Col III was assessed as Col I and Col III mRNA using RT-PCR. Both Col I and Col III mRNA significantly increased after IAV infection during acute and chronic phases (Fig. 5*D*). Myocardial Col I mRNA increased 2.9- to 1.8-fold from *days 9* to *60* postinfection (Fig.

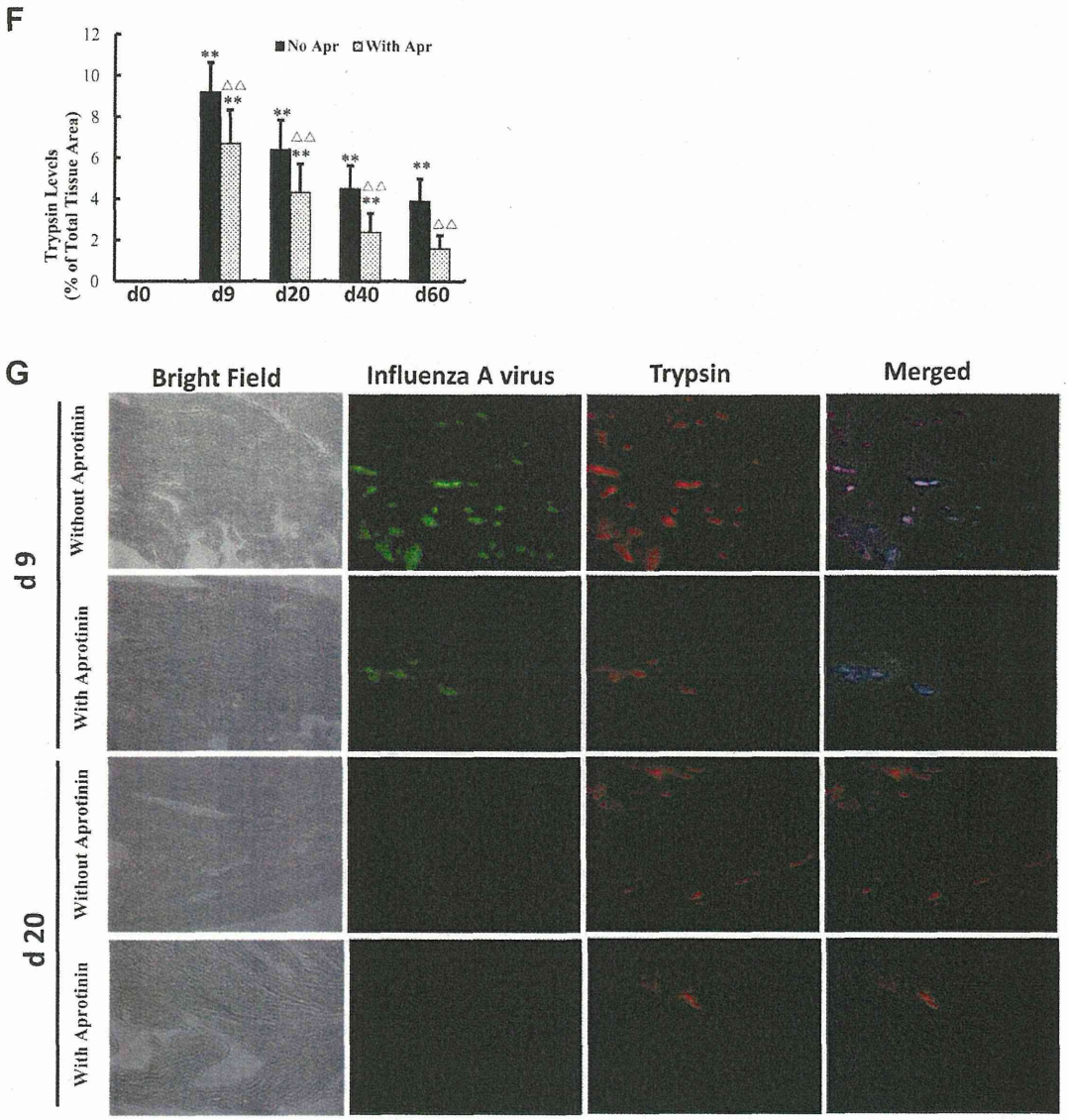

Fig. 2—*Continued*

5*E*). Col III mRNA increased 5.0- to 2.4-fold over the same time (Fig. 5*F*). The differential increase in Col I and Col III led to a decreased Col I-to-Col III ratio in IAV-induced acute and chronic myocarditis (Fig. 5*G*). Aprotinin significantly suppressed collagen upregulation and restored the Col I-to-Col III mRNA ratio.

LV dilation and cardiac dysfunction after IAV infection and effects of trypsin inhibitor. The dynamic changes of cardiac function, LV internal dimension, and LV posterior wall thickness were observed by echocardiography. IAV-infected mice were significantly impaired in LV function, as shown by a significant reduction in FS, EF, SV, and CO and a significant increase in LVESD on *day 9* postinfection, although LVEDD, LVPWd, and LVPWs values were similar to levels on *day 0*. LV function was transiently improved by alleviation of acute myocarditis on *day 20* postinfection and then deteriorated with progressive dilation of LV internal dimension and thinning of LV posterior wall thickness to *day 60* postinfection. Deterioration of cardiac function and dilation of heart chambers were improved significantly by aprotinin with increased values for FS, EF, SV, and CO, reduced values for LVEDD and LVESD, and restored values for LVPWd and LVPWs during acute and chronic myocarditis (Fig. 6 and Table 1).

DISCUSSION

We investigated the pathological mechanisms underlying the development of DCM from IAV-induced myocarditis. First, we found that IAV infection induced a persistent upregulation of ectopic trypsin, which localized in myocardial inflammatory loci, throughout acute and chronic stages. Persistently upregulated trypsin led to continuous activation of proMMP-9 and release of cytokines. Second, myocardial inflammatory infiltration persisted after IAV could not be detected in the myocardium. The severity of myocardial inflammation was consistent with the kinetics of trypsin expression. Third, Col I